A Multilevel Approach to the Minimal Compliance Problem in Topology Optimization *

Roman Stainko
Special Research Program SFB F013
'Numerical and Symbolic Scientific Computing'
Johannes Kepler University Linz
roman.stainko@sfb013.uni-linz.ac.at

Abstract

This paper presents a new solution strategy for a standard topology optimization problem: the minimal compliance problem. This problem contains a partial differential equation (PDE) as a constraint resulting in a large scaled optimization problem after the finite element discretization. Therefore efficient solution techniques pay off, since the computational costs are rather high due to repeated solution of the direct field problem given by the PDE constraint. In this paper we present a new adaptive solution method involving adaptive multilevel techniques. Topology optimization problems are ill-posed, so regularization is needed. In our algorithm we combine two regularization techniques, in fact filter methods, such that their disadvantages are eliminated and only their positive properties remain. Numerical experiments are performed with several benchmark problems, where our multilevel approach turns out to be quite efficient. For solving the optimization problems arising in each iteration step, the method of moving asymptotes is used.
Keywords: Topology Optimization, Minimal Compliance, Filter Methods, Adaptive Mesh-Refinement, Multilevel Approach.

1 Introduction

For the development and design process of new products or structures it is of great importance to find the best possible layout. However it is basically unclear how to choose the initial topology, i.e., where to place material and where to place holes. Also due to the fact that the topology is crucial for finding the optimal layout, it pays off to start the design process with optimizing the basic layout. So it turned out that in the recent decade

*This work has been supported by the Austrian Science Fund 'Fonds zur Förderung der wissenschaftlichen Forschung (FWF)' under the grant SFB F013/F1309.

the field of topology optimization, although it is relatively new, is rapidly expanding with an enormous development in terms of theory, computational methods and applications including commercial applications (e.g., Optistruct by Altair). Often topology optimization is named together with structural optimization, whereas structural optimization is a collective term for topology, shape and thickness optimization. The first is by far the most general as it does not assume the connection of the structural parts, whose shapes and sizes are modified. Shape optimization can, e.g., be seen as a post processing tool after topology optimization, where the shape of the boundary of a product is tuned with respect to some criterion. Thickness optimization is the subject of finding a thickness function so that the resulting design will, e.g., sustain some loads as efficiently as possible. Truss topology problems can be viewed as such a sizing problem. A comprehensive review of these field is given in the monograph by Bendsøe and Sigmund [2] and in the survey articles by Eschenauer and Olhoff [10] and Rozvany [13]. All contain many references on the various aspects of this field of optimization in general.

This paper deals with a multilevel approach to minimal compliance problems. In these problems an optimal material distribution is searched with respect to maximal stiffness and restriction to the total volume used. Minimizing compliance turned out to be a standard problem in topology optimization. However it already contains the most basic, but non-trivial difficulties like mesh dependent solutions, local minima and checkerboard phenomena. The rest of this report is organized as follows. In the next section an introduction to topology optimization by means of minimizing compliance is given. In the following two sections some aspects of topology optimizations are treated, namely material interpolation and regularization. Then, in the next section, our multilevel algorithm is introduced and motivated by the considerations of the previous sections. Also some numerical calculations are presented, which will show the efficiency of the hierarchical approach. In the last section conclusions are drawn and some plans for the future improvements are discussed.

2 The Minimal Compliance Problem

This section gives an introduction to the field of topology optimization on the basis of the so-called minimal compliance problem. That is, how to design the stiffest (or least compliant) structure under a given fixed load, possible support conditions and restriction on the volume of the used material.

The beginning of this section is devoted to the equation that determines the state of equilibrium of a structure under applied external forces. In the following, L_p denotes the L_p spaces ($1 \leq p \leq \infty$) equipped with the norm $\|\cdot\|_{L_p}$, and H^k denotes the Sobolev spaces equipped with the norm $\|\cdot\|_{H_k}$. Details about Sobolev spaces can be found in Adams [1]. Geometric vectors are written in **bold-face** and $|\cdot|$ denotes the Euclidean norm of such a vector. Similarly $\mathbf{L}_p$ and $\mathbf{H}^k$ denote the spaces of vector valued functions which components belong to L_p and H^k respectively.

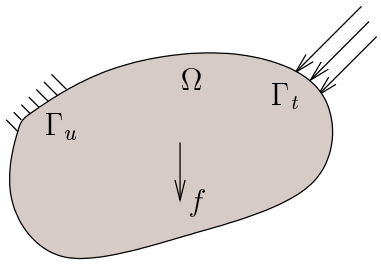

Figure 1: The reference domain and applied forces in a minimal compliance problem.

2.1 The State Equation

Let $\Omega \subset \mathbb{R}^d$ (d = 2,3) be a fixed domain, the so called ground structure. Furthermore Ω is a open, bounded connected domain with a Lipschitz boundary Γ. Moreover let $\Gamma_u \subset \Gamma$, $|\Gamma_u| > 0$ be the part of the boundary where the displacements are fixed, and $\Gamma_t = \Gamma \setminus \Gamma_u$ the part where boundary tractions are predescribed. Later on the optimal design is generated referring to this ground structure.

For describing material in Ω let $\rho \in L^\infty(\Omega)$ be a function representing the material density which fulfills $0 < \underline{\rho} \leq \rho \leq 1$ almost everywhere (a.e.) in Ω, where $\underline{\rho}$ is some positive lower bound. Then, let E^0_{ijkl} describe an elasticity tensor of fourth order, satisfying the usual symmetry, ellipticity and boundedness assumptions, representing a certain isotropic material. Further, let η be a monotonously increasing material interpolation function, mapping $[\underline{\rho}, 1]$ to $(0, 1]$, and describing how the actual density influences the elasticity tensor (e.g., to enforce 'black and white' designs) at a given point $\mathbf{x}$. More information about material interpolation is given in Section 3. Then the actually used elasticity tensor is variable over the ground structure and is defined as

$$E_{ijkl}(\rho(\mathbf{x})) = \eta(\rho(\mathbf{x}))E^0_{ijkl}, \qquad \text{for } \mathbf{x} \in \Omega. \tag{1}$$

Here it is required that $\eta(1) = 1$ and that $0 < \eta(\underline{\rho}) \ll 1$, which describes a very compliant material pretending to be void.

Now for a fixed ρ and for a fixed η, the displacement field $\mathbf{u} \in \mathbf{V}_0$ fulfills the following equilibrium or state equation in its variational formulation:

$$a(\rho; \mathbf{u}, \mathbf{v}) = \ell(\mathbf{v}) \qquad \text{for all } \mathbf{v} \in mathbf{V}_0 \tag{2}$$

where $\mathbf{V}_0 = \{\mathbf{v} \in \mathbf{H}^1(\Omega) \mid \mathbf{v} = \mathbf{0} \text{ on } \Gamma_u\}$ is the space of kinematically admissible displacements. The energy bilinear on $\mathbf{V}_0 \times \mathbf{V}_0$ is defined as

$$a(\rho; \mathbf{u}, \mathbf{v}) = \int_\Omega E_{ijkl}(\rho(\mathbf{x}))\varepsilon_{ij}(\mathbf{u})\varepsilon_{kl}(\mathbf{v})\, d\mathbf{x}, \tag{3}$$

with linearized strains $\varepsilon_{ij}(\mathbf{u}) = \frac{1}{2}\left(\frac{\partial \mathbf{u}_i}{\partial \mathbf{x}_j} + \frac{\partial \mathbf{u}_j}{\partial \mathbf{x}_i}\right)$ and the load linear form

$$\ell(\mathbf{v}) = \int_\Omega \mathbf{f} \cdot \mathbf{v}\, d\mathbf{x} + \int_{\Gamma_t} \mathbf{g} \cdot \mathbf{v}\, ds \tag{4}$$

defines a linear, bounded functional on $\mathbf{V}_0$, where $\mathbf{f} \in \mathbf{L}^2(\Omega)$ defines the body forces and $\mathbf{t} \in \mathbf{L}^2(\Gamma_t)$ describes the boundary tractions.

Again let η be fixed, but ρ arbitrary, then $a(\rho; \mathbf{u}, \mathbf{v})$ satisfies the following conditions (see, e.g., CIARLET [9]):

$$\exists \mu_1 > 0 : \quad \mu_1 \eta(\underline{\rho}) \|\mathbf{v}\|^2_{\mathbf{H}^1(\Omega)} \leq a(\rho; \mathbf{v}, \mathbf{v}), \quad \text{for all } \mathbf{v} \in \mathbf{V}_0, \tag{5}$$

which is due to Korn's inequality, and

$$\exists \mu_2 > 0 : \quad |a(\rho; \mathbf{u}, \mathbf{v})| \leq \mu_2 \|\mathbf{u}\|_{\mathbf{H}^1(\Omega)} \|\mathbf{v}\|_{\mathbf{H}^1(\Omega)}, \quad \text{for all } \mathbf{u}, \mathbf{v} \in \mathbf{V}_0.$$

For the $\mathbf{V}_0$-ellipticity (5) it is crucial that $\eta(\underline{\rho})$ is strictly positive. Assuming that the linear load form $\ell(\mathbf{v})$ fulfills the following boundedness criterion

$$\exists \mu_3 > 0 : \quad \|\ell\|_{\mathbf{V}_0^*} = \sup_{\mathbf{0} \neq \mathbf{v} \in \mathbf{V}_0} \frac{\ell(\mathbf{v})}{\|\mathbf{v}\|_{\mathbf{H}^1(\Omega)}} \leq \mu_3,$$

the total potential energy of the structure, given by a fixed ρ, and the load form ℓ, can be stated as

$$J(\rho; \mathbf{v}) = \frac{1}{2} a(\rho; \mathbf{v}, \mathbf{v}) - \ell(\mathbf{v}).$$

The equilibrium displacement field $\mathbf{u}$ is now the unique minimizer of $J(\rho; \mathbf{v})$ with respect to $\mathbf{v} \in \mathbf{V}_0$, i.e. the principle of minimum potential energy or the principle of virtual work, when equivalently characterized as the solution of (2).

2.2 The Optimization Problem

The considered design problem consists now of minimizing the compliance (maximizing the stiffness) of a structure, with respect to the state equation (2) and some design constraints. For sake of simplicity the body forces in (4) are omitted. Furthermore it is assumed that a proper material interpolation function has been chosen. Mathematically this can be formulated as the following optimization problem:

$$\min_{\rho \in L^\infty(\Omega), \mathbf{u} \in \mathbf{V}_0} \quad \ell(\mathbf{u}) \tag{6}$$

$$\text{subject to:} \quad a(\rho; \mathbf{u}, \mathbf{v}) = \ell(\mathbf{v}) \quad \text{for all } \mathbf{v} \in \mathbf{V}_0, \tag{7}$$

$$\int_\Omega \rho(\mathbf{x}) \, d\mathbf{x} \leq v_0, \tag{8}$$

$$\underline{\rho} \leq \rho(\mathbf{x}) \leq 1 \quad \text{a.e. in } \Omega, \tag{9}$$

Clearly constraint (7) represents the state equation, constraint (8) controls the volume of the used material, where v_0 is a positive bound on the volume used, and (9) ensures that the density stays in reasonable bounds.

In the above formulation the problem would lead to in a simultaneous (all-at-once) approach, reducing the error of the constraining state equation is done at the same time

as minimizing the objective. But usually, and also in this work, the state variable $\mathbf{u}$ is eliminated through (7), resulting in a nested (black-box) approach. For a given admissible ρ the solution of (7) is ensured and then denoted by $\mathbf{u}(\rho)$, arriving at the nested formulation of the minimal compliance problem:

$$\min_{\rho \in L^\infty(\Omega)} \quad \ell(\mathbf{u}(\rho)) \tag{10}$$

$$\int_\Omega \rho(\mathbf{x})\, d\mathbf{x} \leq v_0, \tag{11}$$

$$\underline{\rho} \leq \rho(\mathbf{x}) \leq 1 \qquad \text{a.e. in } \Omega. \tag{12}$$

Now the state constraint (7) is hidden in the objective (10), which means that for every function evaluation or derivative calculation the state equation has to be solved.

Both approaches, the simultaneous and the nested one, have advantages and disadvantages, but it is not within the scope of this report to discuss this, although it is a very interesting subject.

2.3 Discretization using Finite Elements

When solving problems like (6) - (9) or (10) - (12) numerically they are usually discretized using finite elements. For a well funded theory of the finite elements method see, e.g., Braess [7], Brenner and Scott [8] and Grossmann and Roos [11]. Following a standard finite element procedure the ground structure Ω is partitioned into $n = O(h^{-d})$ finite elements τ_i, where h is the used discretization parameter. For a more detailed description of the triangulation we refer to Ciarlet [9]. It is worth noticing that there are two different variables, the displacements $\mathbf{u}$ and the density ρ, but for both the same finite element mesh is used.

The density ρ is approximated by a piecewise constant finite element function $\tilde{\rho}$, i.e. $\tilde{\rho}$ is constant over every finite element τ_i. The displacement field $\mathbf{u}$ is approximated as element-wise quadratic functions and the finite element function $\tilde{\mathbf{u}}$ is now the the unique solution of:

$$a(\tilde{\rho}; \tilde{\mathbf{u}}, \tilde{\mathbf{v}}) = \ell(\tilde{\mathbf{v}}) \qquad \text{for all } \tilde{\mathbf{v}} \in \mathbf{V}_0^h, \tag{13}$$

where $\mathbf{V}_0^h$ illustrates a finite dimensional subspace of $\mathbf{V}_0$. Whenever mesh refinement is performed it is done in such a way that $\mathbf{V}_0^h \supset \mathbf{V}_0^H$ if $h \leq H$. Let the vector $\mathbf{u}^h \in \mathbb{R}^{N_u}$ contain the coefficients of the finite element function $\tilde{\mathbf{u}} \in V_0^h$ and so the discrete analogon of the state equation (2) turns from (13) to the following linear system of equations:

$$\mathbf{K}(\boldsymbol{\rho}^h)\mathbf{u}^h = \mathbf{f}^h \quad \in \mathbb{R}^{N_u}. \tag{14}$$

Here, $\mathbf{f}^h$ denotes the load vector and $\mathbf{K}(\boldsymbol{\rho}^h)$ is the stiffness matrix, depending on the design vector in the form

$$\mathbf{K}(\boldsymbol{\rho}^h) = \sum_{i=1}^{n} \eta(\rho_i^h)\mathbf{K}_i, \tag{15}$$

where $\mathbf{K}_i$ are the element stiffness matrices extended to $N_u \times N_u$ matrices, which are weighted with the values of the material interpolation function evaluated at the elements densities.

Now, with $\mathbf{u}^h(\boldsymbol{\rho}^h)$ denoting the unique solution of (14), the discrete analogon of the continuous objective (10) is ${\mathbf{f}^h}^T\mathbf{u}^h(\boldsymbol{\rho}^h)$. Furthermore let the vector $\mathbf{v}^h$ represent the volumes of the finite elements such that $v_i^h = |\tau_i|$. Then the discrete version of the minimal compliance problem can be posed as follows:

$$\min_{\boldsymbol{\rho}^h \in \mathbb{R}^n} \quad {\mathbf{f}^h}^T(\mathbf{u}^h(\boldsymbol{\rho}^h)) \tag{16}$$

$${\mathbf{v}^h}^T\boldsymbol{\rho}^h \leq v_0, \tag{17}$$

$$\underline{\rho} \leq \rho_i^h \leq 1, \quad i = 1, \ldots, n. \tag{18}$$

3 Material Interpolation Schemes

Actually the basic question in the minimal compliance problem is how to distribute a certain amount of material such that the resulting structure is as stiff as possible. So, for each point of the ground structure one has to decide whether to occupy it with material or not. In this thermology the continuous constraint (12) should be replaced by the discrete version $\rho(\mathbf{x}) \in \{\underline{\rho}, 1\}$ a.e. in Ω. But in order to avoid e.g. branch and bound techniques to solve the discretized '0-1' problem the discrete valued constrained is relaxed and the continuous one is used. However, the design variable is then allowed to attain values between 0 (in fact $\underline{\rho}$) and 1, which is unwanted, and those intermediate values should be penalized to obtain again a more or less 0-1 or 'black and white' design.

By far the most popular penalization method is the so called SIMP (Solid Isotropic Material with Penalization) model, which has turned out to be extremely efficient. Here a nonlinear interpolation model of the form $\eta(\rho(\mathbf{x})) = \rho(\mathbf{x})^p$, with $p \geq 1$ is used, where intermediate values give very little stiffness in comparison to the amount of used material. In other words, by choosing a higher value than 1 for the parameter p, it is inefficient for the algorithm to choose intermediate density values. When minimizing compliance the volume constraint is usually active in the optimal design and computations showed that in this case the optimal layout turns out to be an almost black and white design, if the value of p is high enough, usually $p \geq 3$ is needed. Additionally if one wants to interpret 'grey' areas in the final design as a composite of materials, also $p \geq 3$ is required. Various aspects of interpolation schemes also with respect to material properties can be found in Bendsøe and Sigmund [3, 2]. When a lower bound $\underline{\rho}$ on the density is used, the regions in the optimal design covered by this value can be interpreted as void or as a very compliant material. Following this idea we could see the used material over the ground structure as a composite of two materials, whereas one of those is interpreted as void. If E_0 and E_1 denote the Young's moduli for the two used materials, the Young's modulus of the composite at a point $\mathbf{x}$ is given by

$$E(\rho(\mathbf{x})) = E_0 + \eta(\rho(\mathbf{x}))\triangle E, \tag{19}$$

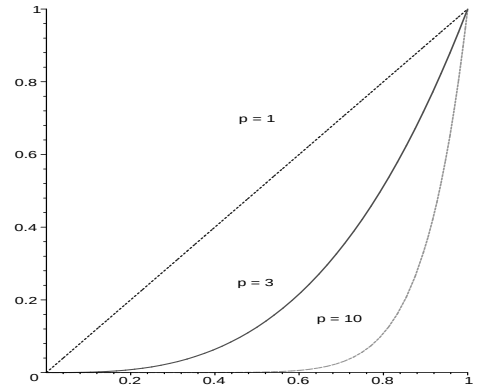

Figure 2: SIMP-Interpolation scheme with various values for p.

where $\triangle E = E_1 - E_0$. Using (19) as the actually used material tensor instead of (1) it is now possible to set $\underline{\rho} = 0$ if it is assumed that $E_1 \gg E_0 > 0$ to ensure the $\mathbf{V}_0$-ellipticity (5) of the bilinear form (3). Furthermore in (15) $\eta(\rho_i^h)$ has to be replaced by $E(\rho_i^h)$. Concerning the Poisson's ratios ν_0 and ν_1 it is assumed that they are the same for both materials. The SIMP interpolation model can then be expressed as

$$E_p(\rho(\mathbf{x})) = E_0 + \rho(\mathbf{x})^p \triangle E.$$

An alternative approach to the SIMP method is the following interpolation model:

$$E_q(\rho(\mathbf{x})) = E_0 + \frac{\rho(\mathbf{x})}{1 + q(1 - \rho(\mathbf{x}))} \triangle E, \tag{20}$$

where $q \geq 0$. This model is called RAMP, which stands for Rational Approximation of Material Properties. One of the advantages of the RAMP model with respect to the SIMP model is the behavior of the derivative of the material model at $\rho(\mathbf{x}) = 0$. Comparing the derivatives yields the following:

$$E_p'(0) = \begin{cases} \triangle E & \text{if } p = 1, \\ 0 & \text{if } p > 0, \end{cases} \quad \text{vs.} \quad E_q'(0) = \frac{1}{1+q} \triangle E > 0,$$

where it is worth noticing that the $E_p'(0)$ is discontinuous in the parameter p, while $E_q'(0)$ is continuous in the parameter q. The fact that $E_p'(0) = 0$ for values of p greater than 1 makes it very hard to move material, which is not the case when using the RAMP model. An other disadvantage of SIMP versus RAMP is that the mass depends linearly on the element density ρ_i^h and the element stiffness depends on the power of ρ_i^h, which results in a non finite ratio of mass to stiffness when ρ_i^h attends zero. More information is given in Bendsøe and Sigmund [2], and a detailed motivation and introduction to the RAMP interpolation scheme can be found in Stolpe and Svanberg [15].

A totally different approach to penalize intermediate density values is to choose the material interpolation function $\eta(\rho(\mathbf{x})) = \rho(\mathbf{x})$ and add an additional constraint to the

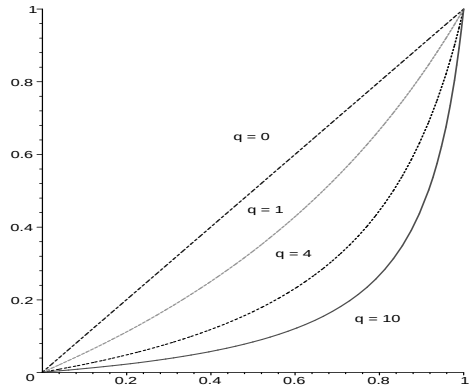

Figure 3: RAMP-Interpolation with various values for q.

optimization problem to encourage 'black-and-white' optimal designs. Such a penalty constraint could e.g. look like the following:

$$P(\rho(\mathbf{x})) = \int_\Omega (1 - \rho(\mathbf{x}))(\rho(\mathbf{x}) - \underline{\rho})\, d\mathbf{x} \leq \varepsilon_P. \tag{21}$$

Of course such a penalty function could also be added as a penalty term to the objective functional.

4 Regularization

A naive formulation of topology optimization tasks like minimizing compliance will lead to difficulties due to the ill-posedness in the sense that there are no optimal solutions. The physical explanation is, that given a structure with a certain volume one can improve the stiffness by introducing a lot of small holes without changing the actual volume, which will lead to an indefinite perforation of the structure. Mathematically speaking the reason for this effect is the non-closeness of the feasible design set.

An optimization problem is said to be well-posed when the two following conditions are valid: The objective functional has to be lower semi-continuous and the feasible set has to be compact, and both properties have to be fulfilled with respect to the same topology. For the minimal compliance problem (10) - (12), the feasible set is weakly* compact in $L^\infty(\Omega)$. However, the objective functional is not weakly* lower semi-continuous in $L^\infty(\Omega)$ when the material interpolation function is chosen according to the SIMP or RAMP technique, in contrast to the original choice $\eta(\rho) = \rho$. But when using $\eta(\rho) = \rho$ and penalizing intermediate values using (21), the set of feasible designs not weakly* closed anymore, see Borrvall and Petersson [5], and the problem lacks solutions again.

The effect that a larger number of holes appears and that more and more fine-scaled parts yield a more detailed structure, when solving the same problem on finer and finer grids, is called *mesh-dependence*. An illustration of the mesh-dependence effect can be seen

in Fig. 4. Ideally refining the mesh should result in the same optimal design, but with a better and smoother description of the boundary. Basically there are two different ways to circumvent the ill-posedness, namely *relaxation methods* and *restriction methods*.

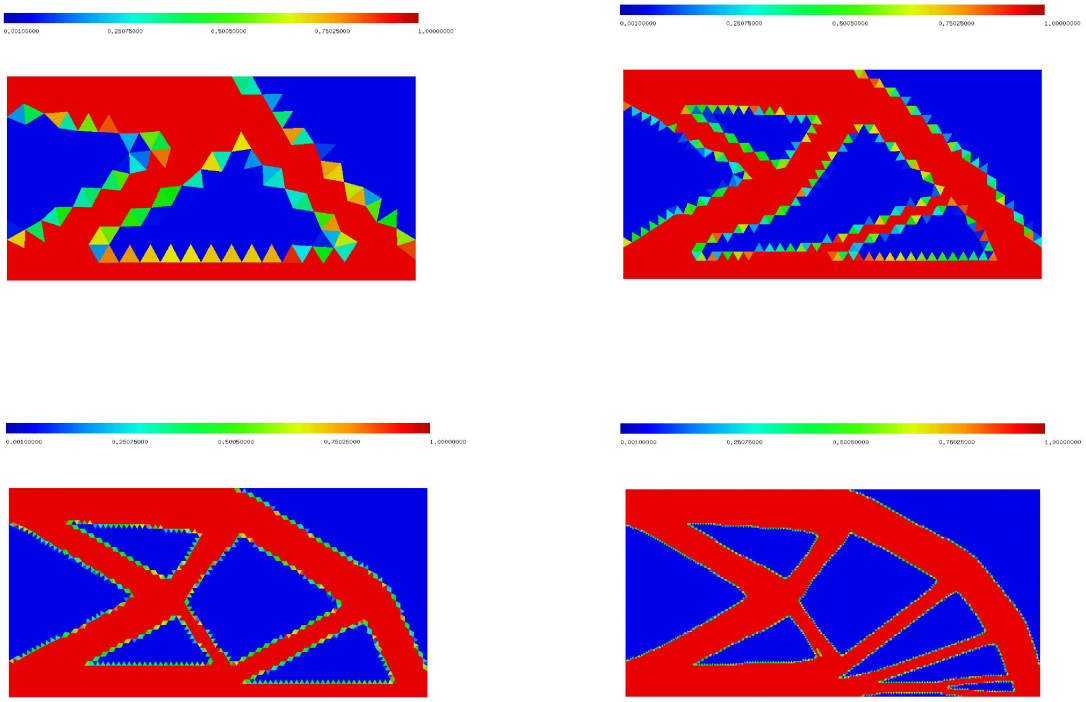

Figure 4: Mesh refinement without regularization. Solutions on a mesh with 449, 1839, 7319, and 29443 elements, respectively.

Relaxation methods in principle enlarge the feasible set of designs. Well-posedness is achieved by introducing an infinitely fine microstructure in every element of the structure and using the homogenized properties of these microstructures as material properties of that element. A deeper insight of this *homogenization approach to topology optimization* is given by, e.g., Bendsøe and Sigmund [2].

In comparison with relaxation methods, restriction methods reduce the set of feasible designs, such that a sufficient closeness is gained. Mainly this is achieved by adding one extra constraint to the problem, ruling out the possibility for fine scale structures to formate, or by using some filter techniques, filtering the sensitivities or directly the density. Summarizations of various restriction methods are given by Bendsøe and Sigmund [2], Sigmund and Petersson [14], Borrvall [4] and Bourdin [6].

Two different filter methods to restrict the design space are used in the calculations presented in this report. The first one is called Regularized Intermediate Density Control (*RIDC*) and is discussed in detail in Borrvall and Petersson [5]. Here the material interpolation function is chosen as $\eta(\rho) = \rho$ such that the problem without any penalization

of intermediate density values is well posed. In the literature this problem is often called the variable thickness sheet. But in order to calculate a black and white optimal design the intermediate density values are penalized by an additional constraint like (21). To get a sufficiently closed set of feasible designs, (21) is modified such that the design variable ρ is filtered firstly by a convolution operator S and then penalized via (21). Let $S : \mathbf{L}^2(\Omega) \to \mathbf{L}^2(\Omega)$ be an integral operator defined as

$$S(\rho(\mathbf{x})) = \int_\Omega \phi(\mathbf{x},\mathbf{y})\rho(\mathbf{y})\, d\mathbf{y},\ \mathbf{x} \in \Omega \quad \text{where} \quad \phi(\mathbf{x},\mathbf{y}) = C(\mathbf{x}) \max\left(0, 1 - \frac{|\mathbf{x}-\mathbf{y}|}{R}\right).$$

$C(\mathbf{x})$ is chosen such that $\int_\Omega \phi(\mathbf{x},\mathbf{y})\, d\mathbf{y} = 1$. Basically this means a linear convolution with a cone of base radius R. The penalizing constraint now looks as the following:

$$P(\rho) = \int_\Omega (1 - S(\rho(\mathbf{x})))(S(\rho(\mathbf{x})) - \underline{\rho})\, d\mathbf{x} \le \varepsilon_P, \tag{22}$$

where a suitable value for ε_p must be found by experiments. Since this procedure is mostly very expensive, this is a serious disadvantage of this approach. But on the other hand for problems like minimal compliance it is mathematically well founded.

The second filter technique is used together with the RAMP interpolation scheme (20). Here not the density, but the discrete element sensivities of an objective J are modified as follows (e.g., see Sigmund and Petersson [14]):

$$\frac{\hat{\partial J}}{\partial \rho_k^h} = \frac{1}{\rho_k^h \sum_{i=1}^n H_{i,k}} \sum_{i=1}^n H_{i,k}\rho_i^h \frac{\partial J}{\partial \rho_i^h}, \tag{23}$$

where the convolution operator $H_{i,k}$ with filter radius R is defined as

$$H_{i,k} = \max\{0, R - \mathrm{dist}(i,k)\}, \quad \text{for } i,k = 1,\ldots,n.$$

The operator $\mathrm{dist}(i,k)$ represents the distance of the geometrical centroids of element k and element i. Roughly speaking this filter replaces the original derivatives by a weighted average of the derivatives of the surrounding area. The advantage of this filter approach is that it is very easy to implement and it turned out to work very well in various different topology optimization problems in 2D and in 3D. Moreover it is very robust with respect to coarse grids. But it must be pointed out that this filter is purely heuristic and it is not quite understood which problem is actually solved. In the following we will call this filter the *mesh-independence filter* and refer to it as *MIF*.

Both filter techniques are able to control the minimal length scale of the components in the optimal design. The larger the filter radius R is, the larger is the minimal length scale or the thicker are the occurring components, which is important, e.g., to ensure that the optimal structure is not to complicated to be manufactured. This influence of the filter radius can be seen Fig. 5.

Another numerical anomaly is the so called *checkerboard effect*, which can be seen in Fig. 6. The appearance of checkerboard patterns is due to bad numerical modeling. For

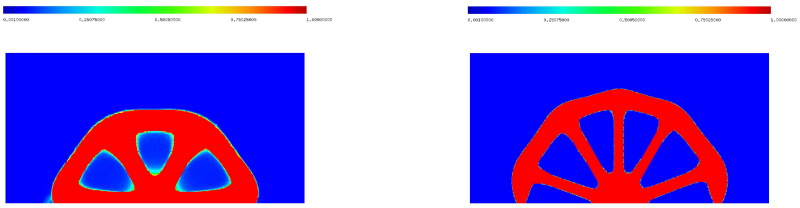

Figure 5: Different sizes of the filter radius: left $R = 0.15$ and right $R = 0.05$.

some combinations of finite element discretizations for the design ρ and the displacements $\mathbf{u}$ these patterns are given an artificial high stiffness when analyzed in their discretized formulation. In the above mentioned citations a detailed explanation and various techniques to prevent these effects are described. Both filters mentioned above have the nice property to remove checkerboard effects or at least reduce them sufficiently.

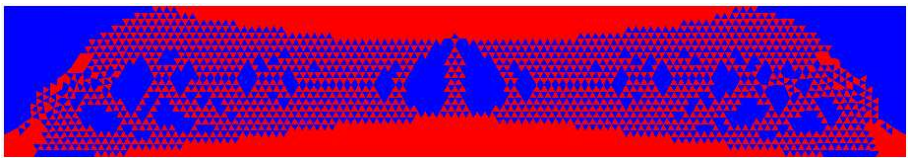

Figure 6: The checkerboard effect in the MBB beam example.

5 Solution Approaches

This section is dedicated to the methods how to solve the discretized problem (16) - (18). For sake of simplicity the index h indicating a discretized variable, like in $\boldsymbol{\rho}^h$, will be omitted in this section, since we only treat the discrete problem anyway.

5.1 Basics of a Convex Programming Method

The problem (16) - (18) is solved iteratively by sequential approximations. We use the so-called *Method of Moving Asymptotes* (MMA) proposed as a successor of its mother method CONLIN by Svanberg [16]. This method is now quite popular in the field of structural optimization. Similar to methods like SQP, at every iteration step, an approximating subproblem is constructed and solved. In MMA these subproblems are convex and separable and rely on gradient information at the given iteration point as well on some information of the latest iterations. The generated subproblem is then solved either by a dual method or by an interior point method. This solution is then used as the actual iterate in the next iteration.

Given an iteration point $\mathbf{x}^{(k)}$ an approximation of a given function f will look like the following: Firstly two parameters $\mathbf{L}^{(k)}$ and $\mathbf{U}^{(k)}$ are chosen, such that

$$L_i^{(k)} < x_i^{(k)} < U_i^{(k)} \quad \text{for } i = 1, \ldots, n.$$

Based on these parameters the approximation $\tilde{f}^{(k)}$ of the given function f is defined as:

$$\tilde{f}^{(k)}(\mathbf{x}) = r^{(k)} + \sum_{i=1}^{n} \left(\frac{p_i^{(k)}}{U_i^{(k)} - x_i} + \frac{q_i^{(k)}}{x_i - L_i^{(k)}} \right), \tag{24}$$

where $r^{(k)}$ and the coefficients $\mathbf{p}^{(k)}$, $\mathbf{q}^{(k)}$ are chosen as

$$\begin{aligned}
p_i^{(k)} &= \begin{cases} \left(U_i^{(k)} - x_i^{(k)}\right)^2 \frac{\partial f}{\partial x_i}(\mathbf{x}^{(k)}), & \text{if } \frac{\partial f}{\partial x_i}(\mathbf{x}^{(k)}) > 0 \\ 0, & \text{if } \frac{\partial f}{\partial x_i}(\mathbf{x}^{(k)}) \leq 0, \end{cases} \\
q_i^{(k)} &= \begin{cases} 0, & \text{if } \frac{\partial f}{\partial x_i}(\mathbf{x}^{(k)}) \geq 0 \\ -\left(x_i^{(k)} - L_i^{(k)}\right)^2 \frac{\partial f}{\partial x_i}(\mathbf{x}^{(k)}), & \text{if } \frac{\partial f}{\partial x_i}(\mathbf{x}^{(k)}) < 0, \end{cases} \\
r_i^{(k)} &= f(\mathbf{x}^{(k)}) - \sum_{i=1}^{n} \left(\frac{p_i^{(k)}}{U_i^{(k)} - x_i^{(k)}} + \frac{q_i^{(k)}}{x_i^{(k)} - L_i^{(k)}} \right).
\end{aligned}$$

The parameters $\mathbf{L}^{(k)}$ and $\mathbf{U}^{(k)}$ act like asymptotes in (24) and control, loosely speaking, the range for which $\tilde{f}^{(k)}$ approximates f reasonably. More details on how to choose the asymptotes and how to generate strictly conservative approximations, can be found in Svanberg [16, 17] and in Bruyneel, Duysinx, and Fleury [12].

The reason why MMA-like methods are popular in topology optimization (combined with a nested approach like in (10) - (12)) is quickly explained. Typically a large number of design variables appears in these problems, since for a good representation of the design one has to work with rather fine finite element meshes and for each element at least one design variable is used, in comparison to a rather small number of constraints. With respect to the large number of design variables the use of SQP methods is very costly if not even impossible, due to the fact that gathering second order information for the approximation of the Hessian could be an insuperable task. Now the two advantageous features of MMA are that the approximating subproblems are convex and separable. Separability means that the necessary conditions of optimality of the subproblem do not couple the design variables, which yields that instead of one n-dimensional problem one has to solve n one-dimensional problems per iteration. Convexity means that dual or primal-dual methods can be used to attack the subproblems. These two valuable properties allow to reduce the computational costs for solving the subproblems significantly.

5.2 A Multilevel Idea

In our multilevel approach we basically tried to combine the two filter methods mentioned in the last section, such that their disadvantages are eliminated and their advantages remain.

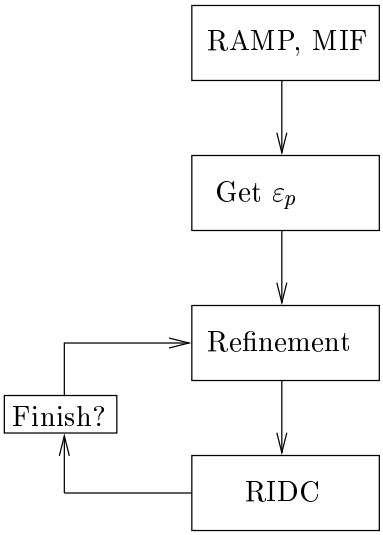

Figure 7: Data flow of our algorithm.

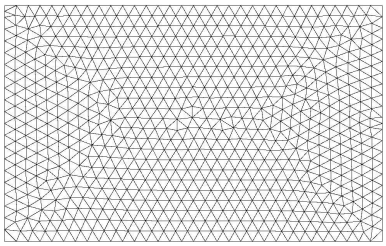

Figure 8: Coarse mesh.

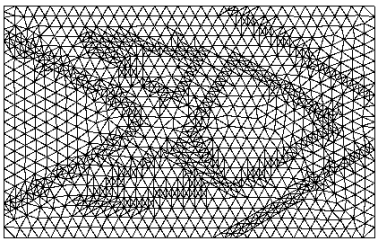

Figure 9: Adaptively refined mesh.

At the beginning the problem is solved on the coarsest grid. Here, at the first level, we use the mesh-independency filter for regularization together with the RAMP interpolation scheme combined with a *continuation method*. The latter means that the RAMP-parameter q is slowly raised through the optimization progress. In the first few iterations $q = q_0$ is chosen, then for next ones some higher value, until a wanted upper value q_{max} for q is reached where the design is finally fully optimized. The advantage of such a continuation method is that one avoids to get early stucked in an unwanted local minima, which may happen if the calculation is done only with one value of q, chosen to large. Since the compliance objective functional (16) is convex for $q = 0$ and concave for $q = \triangle E/E_0$, it is a natural idea to start with $q_0 = 0$ and end with $q_{max} = \triangle E/E_0$, see, e.g., Stolpe and Svanberg [15].

There are two major reasons why we use MIF combined with RAMP on the coarse grid. On the one hand we can use coarser grids as with the RIDC method and on the other hand we use the optimal design $\boldsymbol{\rho}^H$ of the coarse grid to get a realistic value for ε_P in (22), setting $\varepsilon_P = P(\boldsymbol{\rho}_H)$, which saves us costly experiments to find a proper value for ε_P. Although we adapted the MIF formula (23) in an obvious way to work also on unstructured grids, we didn't achieve as good results as on uniform refined grids. So we continue on the refined grids with the RIDC method, which works fine on unstructured grids, is mathematically well-founded and moreover, since the effective density and the original density ρ are the same ($\eta(\rho) = \rho$), there are no doubts which density to plot. The basic data flow of this multilevel approach can be seen in Fig. 7.

So far the adaptive mesh refinement is based on geometrical information gained through identifying elements near the interface between void and material of an optimal design using $\|S(\rho(\mathbf{x})) - \rho(\mathbf{x})\|$ as an indicator. An example of a coarse and an adaptively refined mesh

is shown in Fig. 8 and Fig. 9, respectively.

6 Numerical Experiments

We tested the approach described above with several known benchmark examples and got very good results from all of them. Here we will present results gained from the problems which can be seen in Fig. 10 to 12, where the basic settings, e.g., applied loads and boundary condition, as well the final solutions are shown. We stopped the algorithm when the relative difference of the two latest designs is less then $5 \cdot 10^{-3}$ and the relative difference of two successive objective values is less then $5 \cdot 10^{-5}$ (following BORRVALL AND PETERSSON [5]). For solving the direct problem so far Cholesky factorization is used. The Tables 1 to 4 show the computational data for each example. The columns n_{el}, $n_{\mathbf{u}}$ and n_ρ contain the number of finite elements, the degrees of freedom w.r.t. the displacements and the degrees of freedom w.r.t. the density, respectively. The other columns t_{state}, t_∇, t_{opt} and t_{it} show the time used for one evaluation of the state equation, of the derivatives, for the solution of the subproblem and the time for one whole iteration, respectively. The difference in time between t_{it} and the other three columns is mainly used for applying the filter, which is done recursively. In the last column the number of iterations is listed. The last lines in these tables always show the data of the experiments where we did the computations on only one uniform mesh, where the elements were of the size of the smallest ones of the mesh in level 4, which gives an impression about the gained speedup.

	n_{el}	$n_{\mathbf{u}}$	n_ρ	t_{state}	t_∇	t_{opt}	t_{it}	*Iter.*
level 1:	1352	5694	1352	0.8	0.4	0.01	1.3	171
level 2:	2848	13180	2848	2.0	0.8	0.02	2.9	31
level 3:	8428	41116	8428	8.0	2.3	0.07	11.3	14
level 4:	17666	87336	17666	22.7	4.8	0.15	33.4	10
level 5:	37536	186716	37536	48.4	10.2	0.38	103.3	8
direct:	88559	356484	88559	573.1	24.9	1.07	978.3	152

Table 1: Computational data from the MBB beam problem.

7 Conclusions and Outlook

In our multilevel approach we combined two filter techniques such that their disadvantages are eliminated and we gain from their good properties. Finally we ended up with an efficient method to solve minimal compliance problems with a high resolution of elements around the interface between void and material.

So far only numerical examples in 2D are presented, but the code is written such that the step to *3D computations* can be done without too much effort. Another point of

	n_{el}	$n_{\mathbf{u}}$	n_ρ	t_{state}	t_∇	t_{opt}	t_{it}	$Iter.$
level 1:	1852	7654	1852	1.7	0.5	0.01	2.3	143
level 2:	3283	14824	3283	3.7	0.9	0.02	4.8	48
level 3:	8255	39744	8255	12.4	2.2	0.05	15.9	28
level 4:	16639	81694	16639	28.2	4.5	0.10	37.8	21
level 5:	37992	188522	37992	60.0	10.3	0.21	120.1	15
direct:	117695	472704	117695	1498.7	33.2	0.81	2109.1	135

Table 2: Computational data from the wheel example.

	n_{el}	$n_{\mathbf{u}}$	n_ρ	t_{state}	t_∇	t_{opt}	t_{it}	$Iter.$
level 1:	449	1920	449	0.2	0.1	0.01	0.4	119
level 2:	1016	4758	1016	0.6	0.3	0.01	1.0	32
level 3:	2843	13926	2843	2.4	0.8	0.02	3.4	23
level 4:	6136	30424	6136	5.7	1.7	0.04	8.5	13
level 5:	11652	58028	11652	13.0	3.2	0.08	23.1	8
direct:	29443	118736	29443	147.3	8.3	0.20	186.7	113

Table 3: Computational data from the first cantilever beam problem.

	n_{el}	$n_{\mathbf{u}}$	n_ρ	t_{state}	t_∇	t_{opt}	t_{it}	$Iter.$
level 1:	1463	6068	1463	1.2	0.4	0.01	1.6	103
level 2:	2761	12564	2761	2.7	0.8	0.03	3.6	24
level 3:	7624	36924	7624	9.3	2.1	0.08	12.2	13
level 4:	17164	84684	17164	25.3	4.6	0.20	35.9	9
level 5:	36954	183168	36954	56.2	10.0	0.47	117.9	7
direct:	94066	377934	94006	1211.9	26.1	1.31	1626.3	89

Table 4: Computational data from the second cantilever beam problem.

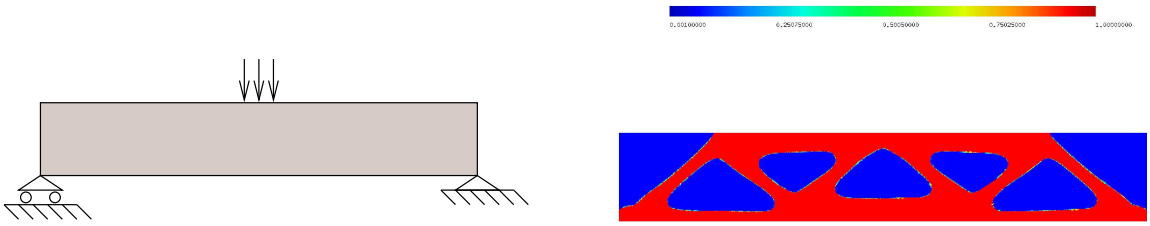

Figure 10: The MMB beam example, $R = 0.1$, volume fraction 0.5, measurements: 6×1.

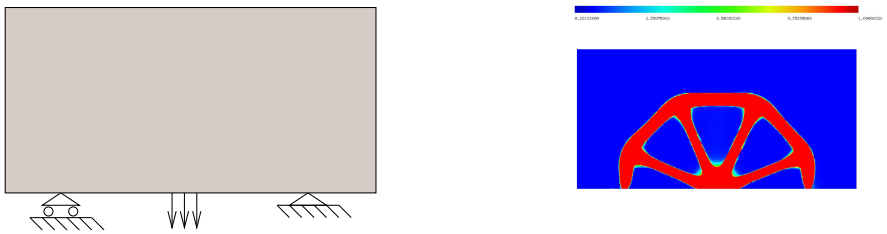

Figure 11: The half of a wheel, $R = 0.1$, volume fraction 0.2, measurements: 4×2.

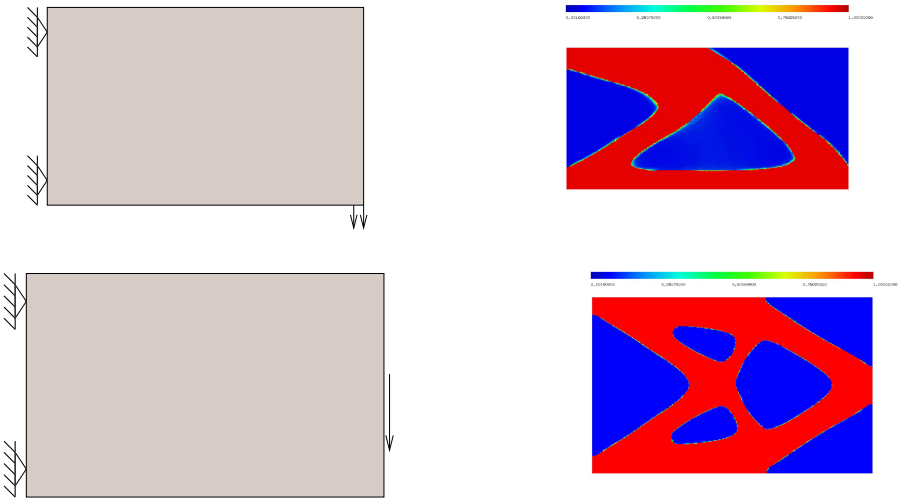

Figure 12: Two cantilever beam examples, $R = 0.1$, volume fraction 0.5, measurements 2×1 and 3.2×2.

high interest is also the upgrade of the solver for the direct field problem from Cholesky factorization to a *multigrid preconditioned conjugate-gradient method*. Since we already have a hierarchy of solutions on different grids it is natural to use a multigrid method for solving the direct field problem. Moreover, for an efficient use of multigrid methods some difficulties have to be overcome. For instance, a tricky and non-trivial problem will be the handling of the interface between void and material form level to level. In order to describe

the this interface more precisely so far only local h-refinement is done. However this leads to a large number of elements and variables, respectively. Consequently, the usage of an adaptive hr-method including mesh-unrefinement will be an effective alternative strategy. Moreover, the application of the MIF method to unstructured grids is also a desirable goal.

But despite all this plans concerning the nested approach to minimal compliance (topology optimization) problems, the final aim is to combine all the above improvements with a *simultaneous approach*, which will be a very challenging task.

References

[1] R.A. Adams. *Sobolov Spaces*. Academic Press, New York, 1976.

[2] M. P. Bendsøe and O. Sigmund. *Topology Optimization: Theory, Methods and Applications*. Springer, Berlin, 2003.

[3] M.P. Bendsøe and O. Sigmund. Material interpolation schemes in topology optimization. *Archive of Applied Machincs*, 69:635–654, 1999.

[4] T. Borvall. Topology optimization of elastic continua using restriction. Technical report, Department of Mechanical Engineering, Linköpings Universitet, Linköping, Sweden, 2001.

[5] T. Borvall and J. Petersson. Topology optimization using regularized intermediate density control. Technical report, Department of Mechanical Engineering, Linköpings Universitet, Linköping, Sweden, 2000.

[6] Blaise Bourdin. Filters in topology optimization. *International Journal for Numerical Methods in Engineering.*, 0:1–17, 2000.

[7] D. Braess. *Finite Elements: Theory, Fast Solvers and Applications in Solid Machanics*. Cambridge University Press, 1997.

[8] S.C. Brenner and L.R. Scott. *The Mathematical Theory of Finite Element Methods*. Springer, New York, 1994.

[9] P. G. Ciarlet. *The Finite Element Method for Elliptic Problems*. North-Holland, Amsterdam, 1978.

[10] H.A. Eschenauer and N. Olhoff. Topology optimization of continuum structures: A review. *Applied Machanics Rev*, 54(4), 2001.

[11] Ch. Großmann and H.-G. Roos. *Numerik partieller Differentialgleichungen*. B.G. Teubner, Stuttgart, 1994.

[12] P. Duysinx M. Bruyneel and C. Fleury. A family of mma approximations for structural optimization. *Structural and Multidisciplinary Optimization*, 24:263–276, 2002.

[13] G.I.N. Rozvany. Aims, scope, methods, history and unified terminology of computer-aided topology optimization in structural mechanics. *Structural and Multidisciplinary Optimization*, 21:90–108, 2001.

[14] O. Sigmund and J. Petersson. Numerical instabilities in topology optimization: A survey on procedures dealing with checkerboards, mesh-dependencies and local minima. *Structural and Multidisciplinary Optimization*, 16:68–75, 1998.

[15] M. Stolpe and K. Svanberg. An alternative interpolation scheme for minimum compliance topology optimization. *Structural and Multidisciplinary Optimization*, 22:116–124, 2001.

[16] K. Svanberg. The mthod of moving asymptotes - a new method for structural optimization. *International Journal for Numerical Methods in Engineering*, 24:359–373, 1987.

[17] K. Svanberg. A class of globally convergent optimization methods based on conservative convex separable approximations. *SIAM Journal of Optimization*, 12(2):555–573, 2002.